

## Results of a magnetic-monopole search utilizing a large-area proportional-tube array

K. N. Buckland, G. E. Masek, W. Vernon, L. M. Knapp, and J. P. Stronski

*Department of Physics, B-019, University of California—San Diego, La Jolla, California 92093*

(Received 26 October 1989; revised manuscript received 15 February 1990)

The results of a recent magnetic-monopole search are presented. The detector is an array of He-CH<sub>4</sub> proportional tubes whose effective area–solid-angle product is 265 m<sup>2</sup>sr. For a live time of 578 days, no bare monopole candidates were observed, setting an upper flux limit of  $1.8 \times 10^{-14}$  cm<sup>-2</sup>sr<sup>-1</sup>s<sup>-1</sup> (90% C.L.) for  $\beta > 1.1 \times 10^{-4}$ .

### I. INTRODUCTION

The discovery by 't Hooft and Polyakov<sup>1</sup> that the existence of magnetic monopoles are a necessity in grand unified theories (GUT's) that contain an unbroken U(1) symmetry has spawned an increase in experimental searches for these particles. The GUT monopole is expected to be massive  $\sim 10^{16}$  GeV and have velocities ranging from those typical of Earth-bound orbits  $\sim 10^{-5}$  c, up to the escape velocity of the galaxy or local supercluster  $\sim 10^{-3}$  c. Numerous experiments have been completed using a variety of detection techniques;<sup>2</sup> however, with the possible exception of Cabrera's event,<sup>3</sup> no viable monopole candidate has been observed.

Turner, Parker, and Bogdan<sup>4</sup> have used the interaction of monopoles with the galactic magnetic field and energy-conservation arguments to provide an astrophysical bound for the monopole flux. The actual limit depends upon the mass, as well as the velocity of the monopole, but the most likely bound is  $\Phi < 10^{-15}$  cm<sup>-2</sup>s<sup>-1</sup>sr<sup>-1</sup> for masses of  $10^{16}$  GeV and  $v \sim 10^{-3}$  c. To effectively probe flux levels of this magnitude, it is necessary to use large-area detectors. While the induction devices are essentially velocity independent and provide unambiguous signals, their ability to cover large areas is currently quite limited.<sup>5</sup> Scintillators have provided large-area coverage,<sup>6,7</sup> and theoretical predictions due to Ahlen and Tarlé<sup>8</sup> indicate that the monopole should provide signals down to a distinct cutoff in energy loss at  $6.7 \times 10^{-4}$  c. In fact, recent experiments<sup>9</sup> have shown scintillation response to protons with velocities approaching  $2.5 \times 10^{-4}$  c, with no indication of any kinematic cutoff. This suggests the possibility that scintillator arrays could be sensitive to monopoles with velocities lower than the cutoff predicted by the models.

An alternative energy-loss mechanism for monopoles in He and H<sub>2</sub> has been calculated by Drell, Kroll, Mueller, Parke, and Ruderman<sup>10</sup> (DKMPR), which provides a means of extending the detectable velocities down to  $v \sim 10^{-4}$  c. In this mechanism, the monopole passes near the atom and induces atomic transitions from the ground state to an excited metastable state. If proper gases (e.g., CH<sub>4</sub> or CO<sub>2</sub>) are also present in the mixture, they will be ionized with high efficiency<sup>11</sup> by collisions with the excited atoms (Penning effect), thus allowing the use of large proportional-chamber arrays for detection of monopoles.

A more recent calculation<sup>12</sup> lowers the expected energy loss in He by 30% from that originally reported by DKMPR, and is shown in Fig. 1.

Studies on the formation and dissociation of monopole-proton bound states in the early Universe<sup>13</sup> have implied that at the end of the hot era (recombination temperature) the majority of monopoles may be bound to protons. The actual percentage of bound states is crucially dependent upon the ground-state energy of the system and likely values can be as low as 60% (Ref. 14). The charge carried by the bound proton can affect the energy-loss characteristics of the state; thus detectors operating on energy-loss mechanisms must distinguish between bare monopoles and positively charged dyons.

### II. DESCRIPTION OF DETECTOR

The detector described here is a larger version of a prototype instrument, the results of which have been reported previously.<sup>15</sup> The apparatus (shown in Fig. 2) consists of 2304 independent proportional tubes arranged in 12 planes of 192 tubes each. The tubes within eight of the planes are oriented in the North-South (N-S) direction, while those of the remaining four are orthogonal. The Al tubes have an inner diameter of 3.5 cm and are 7.3 m in length. Each tube is strung with 51- $\mu$ m-diameter Au-

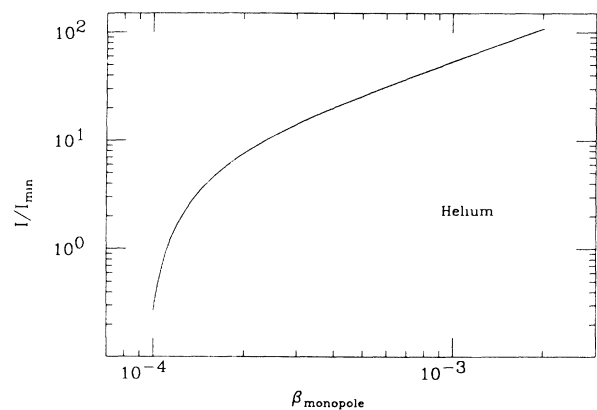


FIG. 1. Energy loss (in units of  $I/I_{\min}$ ) vs  $\beta$  for bare magnetic monopoles in He through DKMPR (see text) mechanism. The curve shown here is from the most recent calculation of Ref. 12.

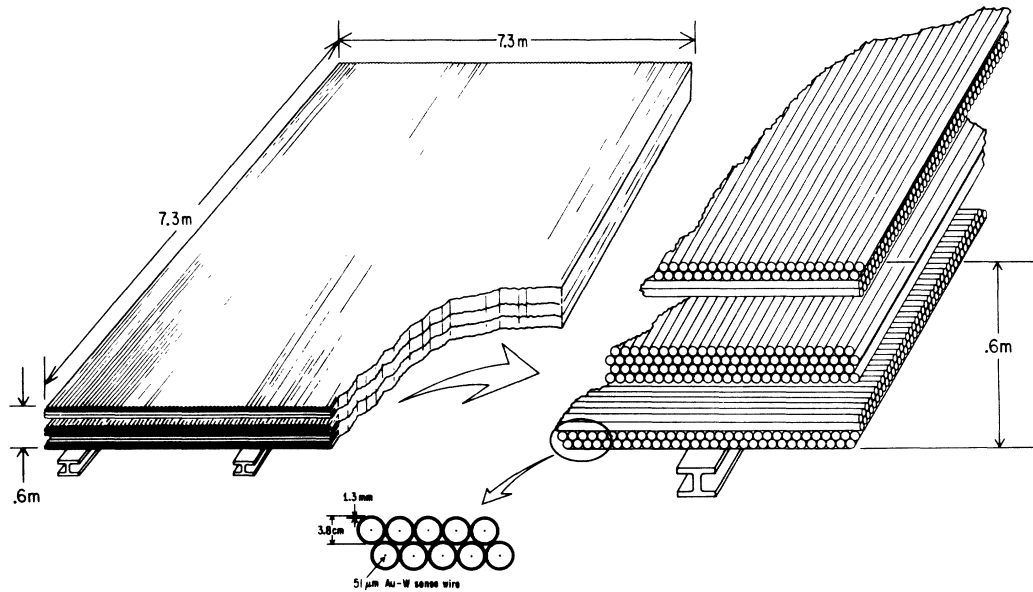


FIG. 2. Configuration of the monopole detector array. Note that the tubes in four of the planes are oriented orthogonal to the tubes in the main body of the array. Also shown are the individual proportional-tube cross sections, and the associated offset in the tube positions used to decrease the possibility of "dead" areas within the array.

plated tungsten wire, and a potential difference of 2150 V is applied. The vertical separation of the outside planes is 0.6 m; hence the detector subtends an effective area-solid angle product (acceptance) of 265 m<sup>2</sup>sr. The tubes are filled with a mixture of He-CH<sub>4</sub>-H<sub>2</sub> (80-19-1) at 1 atm, and a 15–20 ft<sup>3</sup>/h flow rate is maintained. The gas quality can be monitored at various points within the system using standard gas chromatography, and has been held to close tolerances throughout the experiment.

Outputs from each of the 2304 channels are first amplified (gain ~ 150, integrating time ~ 0.5 μs) and then individual comparators select a minimum signal threshold. The actual pulse heights are not recorded but rather the time duration (width) of the signal above threshold. These pulse widths are then related logarithmically to the

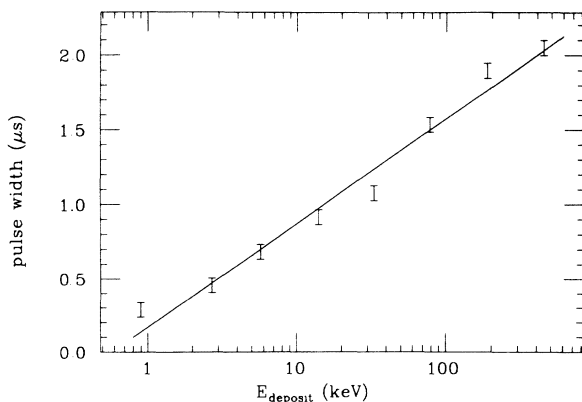


FIG. 3. Pulse width recorded vs equivalent energy deposited by a burst of photoelectrons within the tube. The data was obtained by using a pulsed N<sub>2</sub> laser of variable intensity to produce the photoelectrons and comparing the resulting pulse heights (widths) to that produced by an <sup>55</sup>Fe source.

pulse heights. The height-width calibration was obtained by both injecting appropriately shaped pulses directly on the individual sense wires and by varying the high voltage (gain) while observing pulses produced by a radioactive source.

It is desirable that the tubes operate within the proportional mode and remain linear in response over a wide range of incident ionization. The self-induced space-charge effect has been shown<sup>16</sup> to affect gas gain in such tubes, and a related phenomena of gas gain dependence on incident angle of heavily ionizing particles<sup>17</sup> has been established. Hence, the proportional-tube response was checked by using a pulsed N<sub>2</sub> laser ( $\lambda = 337$  nm) to produce a burst of photoelectrons within the cell while observing the output signal characteristics (pulse height and width) as the laser intensity was varied. The equivalent energy calibration was obtained by comparing the laser-induced pulse heights to that produced by an <sup>55</sup>Fe source (conversion of 6.5-keV x ray). As shown in Fig. 3, the tube response remains linear to at least 500 keV of equivalent energy deposit. The tubes respond differently to penetrating particles that produce an extended track of primary ionization through the tube (cosmic-ray muons,  $\alpha$  particles, and possible monopoles). In this case, a typical drift time within the tube (1 μs) is on the order of the integration time of the amplifier (0.5 μs) and different segments of the primary ionization track will arrive at different times to the amplification region near the anode wire. This results in a mechanism of pulse broadening for penetrating particles that is negligible for the photoelectrons used in the energy calibration. Thus, the energy calibrations discussed above are not directly applicable for the penetrating particles of interest, and were used solely to guarantee the proportional-tube response linearity. The actual energy calibration of the array was refer-

enced back to a minimum-ionizing particle (cosmic-ray muon) passing through the complete array. The triggering system, filters, and analysis of events make use of this well-established cosmic-ray muon signal of  $1.2 \mu\text{s}$  (averaged over all planes). Recalling that the pulse width is a logarithmic measure of the pulse height or ionization deposited within a tube, the minimum-ionizing muon signal can be used to determine a detector ionization threshold of  $0.09I_{\text{min}}$ .

The output of each comparator is split, half forming logical sums of all signals in individual planes to be used in triggering electronics, and the other half feeding directly to memory modules for data acquisition. In the memory modules the separate channels are recorded on  $1024 \times 8$  RAMs whose addresses are incremented at 10 MHz. The information stored on the RAM system (plane number, wire number, time, and width) is read out when an appropriate signal from the trigger electronics is received.

The detector is operated at sea level with no Earth overburden, and thus must rely upon electronic rejection to eliminate the large cosmic-ray muon background. The detector transit time expected of slow-moving monopoles will make these signals easy to distinguish from the fast muon component, and the higher specific ionization expected of higher velocity monopoles will stand out against the minimum ionization of cosmic-ray muons.

A Monte Carlo study of various triggering schemes indicated that the highest monopole acceptance was obtained with a three component trigger system with timing and coincidence values as listed below. The components are labeled as slow, medium, and fast, depending upon the velocity region which is favored by each. Only the N-S planes (numbered 1–8 from the top) are used in the trigger, with the orthogonal East-West (E-W) planes (9–12) used for track reconstruction only. The triggering system divides the detector into two independent halves, with each half triggering the entire complement of E-W tubes.

The slow trigger relies upon signal timing properties to identify the passage of slowly moving particles through the array which deposit  $I > I_{\text{threshold}}$  in at least seven of the eight trigger planes. The following criteria are imposed: (i) Events are rejected if the time differences between any two of the four pairs (1-2, 3-4, 5-6, 7-8) are less than  $0.4 \mu\text{s}$ ; (ii) events are rejected if any five planes have hits within  $0.7 \mu\text{s}$ ; (iii) seven planes must have recorded a hit within  $35 \mu\text{s}$ ; (iv) the time difference between outer

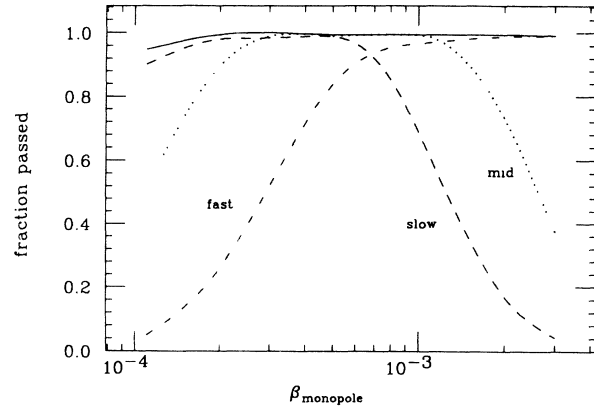


FIG. 4. Monte Carlo performance of tricomponent triggering system (see text). The acceptance of the various trigger components are plotted against the velocity of Monte Carlo-generated monopole tracks. The solid line represents the acceptance of the full trigger logic.

pairs (1-2, 7-8) must be greater than  $0.7 \mu\text{s}$ ; (v) the event must contain seven or more planes.

The medium trigger also relies upon signal timing properties and is, in fact, a relaxed version of the slow trigger discussed above. The following criteria are imposed: (i) events are rejected if any five planes have hits within  $0.7 \mu\text{s}$ ; (ii) seven planes must have recorded a hit within  $15 \mu\text{s}$ ; (iii) the time difference between outer pairs must be greater than  $0.7 \mu\text{s}$ ; (iv) the event must contain seven or more planes.

Whereas the slow and medium triggers rely upon signal timing properties, the fast trigger makes use of the larger pulse height (width) for higher velocity monopoles (recall Fig. 1). The fast trigger requires that the pulse width be greater than  $2.3 \mu\text{s}$  in at least seven of the eight trigger planes, and no timing constraints are imposed.

A Monte Carlo calculation of the trigger performance is shown in Fig. 4, which displays the acceptance as a function of the monopole velocity for the full trigger, as well as the individual components. Note that the slow trigger acceptance (as well as the full trigger) will fall off rapidly below  $\beta = 1.1 \times 10^{-4}$  as  $I/I_{\text{min}}$  approaches (recall Fig. 1) the threshold value of 0.09. The medium trigger effectively “fills in the gap” between the slow and fast trigger acceptance. As shown in Table I, which depicts the rates that are present at various stages of the data-acquisition system, the trigger system is reasonably

TABLE I. Rates present at various stages of the data acquisition and analysis.

Stage	Rate	Rate (normalized to CR)
Cosmic-ray rate (CR) throughout array	8.0 kHz	1
Hardware trigger	0.66 Hz	$8.2 \times 10^{-5}$
SBC software cuts	0.26 Hz	$3.2 \times 10^{-5}$
VAX on-line filters	280/day	$4.1 \times 10^{-7}$
Tracking filter	17/day	$2.4 \times 10^{-8}$
DKMPR (see text) filter	3/month	$1.4 \times 10^{-10}$

effective at rejecting cosmic-ray tracks.

When the appropriate conditions are met in the hardware trigger electronics, the data stored in the memory modules is read out through three Cromemco single-board computers (SBC's) and sent to a VAX Station 2000 for further on-line data analysis and filtering. The VAX also provides a wide selection of diagnostic histograms from which the overall system performance can be monitored. The SBC itself provides for additional software triggering by requiring that at least three of the four pairs of trigger planes contain at least one "cluster." A cluster is defined such that a hit in a tube of the first plane is accompanied by another hit in at least one of the adjacent tubes in the second plane making up the pair. This condition must hold for any real track within the array and is the first attempt to identify actual tracks within the event. Also, in order to avoid complicated and noisy events, the event must contain less than 100 hits in the 12 planes. In this manner the SBC provides another 50% reduction in the data rate transmitted to the VAX.

In the VAX, the events are filtered online through a pattern recognition and track fitting routine which uses the cluster and timing information to identify track candidates. Selected track candidates must satisfy the following requirements.

(i) At least one of the hits associated with the track must be identified with the original trigger timing sequence, since many events contain several tracks.

(ii) The track must begin in pairs (1-2) or (7-8) and end in pairs (7-8) or (1-2) corresponding to a particle traversing the complete detector in either direction.

(iii) The average times of each cluster within the track must be increasing or decreasing from top to bottom in the array, which is consistent with a slowly moving particle passing through the detector.

(iv) The transit time of the track must be greater than 1  $\mu$ s.

In addition, tracks which contain seven or more planes with widths greater than 2.3  $\mu$ s (heavily ionizing) are also passed through the filter, regardless of timing signatures. These constraints on individual tracks are consistent with the trigger conditions held on the detector planes. This results in  $\sim 280$  events/day being written to disc (see Table I).

### III. ANALYSIS OF DATA

In the off-line analysis, the events are passed through a more sophisticated tracking filter which uses a variety of linear fits to extract those track candidates which satisfy a "good" fit criteria. A fit to the mean projected position of the hits in the N-S tubes of each plane participating in the track candidate ( $\bar{X}_i$ ) gives a fit position ( $X_i$ ) and a quantity  $\sigma_x^2$  is defined such that

$$\sigma_x^2 = \frac{1}{n-2} \sum_{i=1}^n (X_i - \bar{X}_i)^2,$$

where  $n$  is the number of planes containing hits within the track ( $n > 6$ ). Similarly, a fit to the mean times of hits within each pair versus the projected distance along

the track in each of the  $n$  planes ( $T_j$ ) gives a fit time ( $t_j$ ) and

$$\sigma_t^2 = \frac{1}{n-2} \sum_{j=1}^n (T_j - \bar{T}_j)^2.$$

The  $\sigma^2$  values can be used to screen out false tracks generated by the track fitting routine, incomplete and noisy tracks such as multiple close proximity tracks (showers), and  $\mu$ - $e$  decays occurring within the array. Monte Carlo studies were used to determine the  $\sigma^2$  values of monopole tracks within the velocity range of interest. In this manner,  $\sigma^2$  cuts were chosen such that a 99.6% monopole acceptance was obtained. A track candidate must lie within the  $\sigma^2$  window of  $\sigma_x^2 < 2.7 \text{ cm}^2$  and  $\sigma_t^2 < 30$  ( $0.1 \mu\text{s}^2$ ). Figure 5 shows a portion of a scatter plot of  $\sigma_x^2$  vs  $\sigma_t^2$  for those events which have passed the on-line filter requirements of a typical data run. The  $\sigma^2$  acceptance window defined above is shown as the small box at lower left in the figure. The window parameters accept  $\sim 25\%$  of the events in the data sample indicated. The inset at upper right depicts a blowup of the  $\sigma^2$  window and shows the fit results of 1200 Monte Carlo monopoles evenly distributed over the velocity range of  $1.1 \times 10^{-4} \leq \beta \leq 10^{-3}$ . The  $\sigma^2$  window parameters can be checked independently by using a cosmic-ray trigger and observing that the muon tracks also cluster within the window chosen above. Finally, for those events which remain, hits in the East-West (E-W) tubes which are within the proper time window determined for the track are considered. As before, a fit to the mean projected position of the hits in the E-W tubes ( $\bar{Y}_k$ ) gives a fit position ( $Y_k$ ) and

$$\sigma_y^2 = \frac{1}{m-2} \sum_{k=1}^m (Y_k - \bar{Y}_k)^2,$$

where  $m$  is the number of E-W planes containing hits within the track ( $m = 3$  or  $4$ ). A track candidate must have  $\sigma_y^2 < 3.4 \text{ cm}^2$  to be passed. Roughly 17 events/day survive at this point (see Table I).

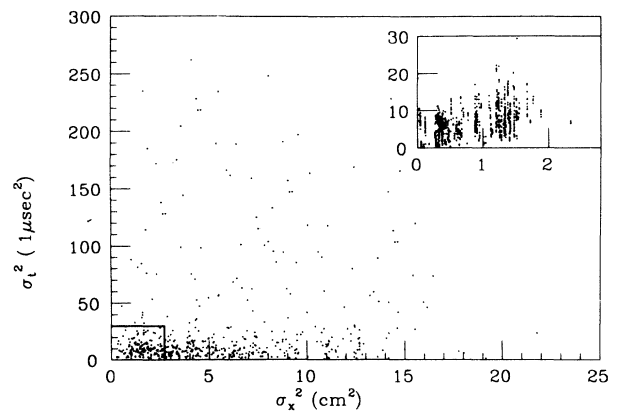


FIG. 5.  $\sigma_x^2$  vs  $\sigma_t^2$  for events which satisfy the on-line filter requirements. The  $\sigma^2$  acceptance window (discussed in the text) is shown at lower left and accepts  $\sim 25\%$  of the data sample. The inset shows the fit results of 1200 Monte Carlo monopoles distributed over the velocity range of  $1.1 \times 10^{-4} \leq \beta \leq 10^{-3}$  and indicates  $> 99\%$  acceptance.

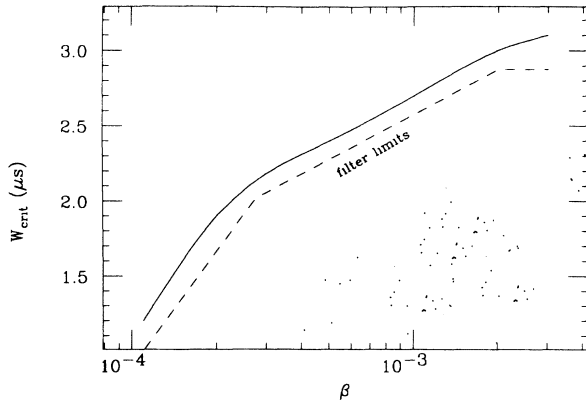


FIG. 6. Critical pulse width (see text) vs monopole velocity (in units of  $v/c$ ) as determined from Monte Carlo simulation (solid curve) and as used in the off-line software filter (dashed lines). The scattered points represent a data sample of low-velocity tracks which have survived to this point of the analysis.

At this stage of the analysis, the data was analyzed for bare monopoles with the question of possible dyons not being addressed in this paper. For free monopoles use is made of the DKMPR energy-loss mechanism. A Monte Carlo generation of 3000 monopole tracks ( $1.1 \times 10^{-4} \leq \beta \leq 3 \times 10^{-3}$ ) satisfying DKMPR criteria was used to determine the average pulse width  $\bar{W}$  within the track as a function of velocity. A critical pulse width  $W_{\text{crit}}$  was defined at each velocity such that 99.99% of the Monte Carlo monopoles had  $\bar{W} > W_{\text{crit}}$ . Figure 6 shows  $W_{\text{crit}}$  as a function of velocity, as well as the “relaxed” filter requirements which were actually used. Thus, the implied velocity is determined for each track candidate, and the average pulse width of the signals comprising the track is required to exceed the filter requirements shown in the figure. The scattered points in Fig. 6 represent a data sample of low-velocity tracks which have passed through the various filters (notably those within the  $\sigma^2$  window of Fig. 5) and survived to this point of the analysis. As seen in the figure, the distribution of implied track velocities decreases rapidly towards

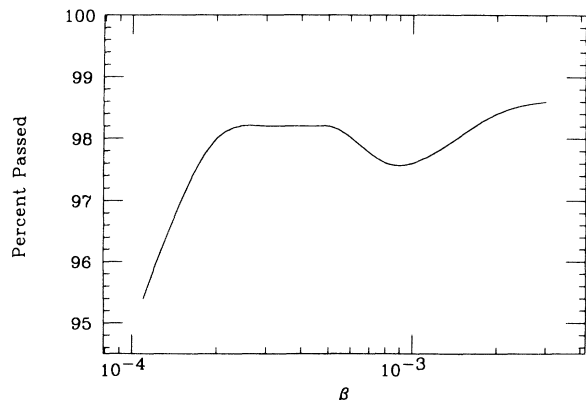


FIG. 7. The acceptance of the “total” filter (see text) as a function of monopole velocity (in units of  $v/c$ ) determined from Monte Carlo studies.

TABLE II. The classification (as described in the text) after visual scanning of the 190 events which survived the complete filtering process.

Classification	Observed number	Fraction of total
Multi-CR	86	0.45
Showers	52	0.27
Skew-CR	42	0.22
Overlap-CR	8	0.04
Malfunction	2	0.01

the lower velocities, and the DKMPR energy-loss mechanism provides an extremely useful filter criteria for those tracks which remain. At this point, roughly three events/month survive, while the Monte Carlo acceptance is  $\approx 98\%$  (see Fig. 7).

To date, 190 events have survived the complete filtering process and have undergone visual scanning. All of the events have been identified as fast triggers (large pulse widths) and classified as shown in Table II. “Multiple cosmic rays” are events in which two or more cosmic rays pass through the same N-S tubes in each layer within a time window defined by the typical cosmic-ray pulse width of  $1.2 \mu\text{s}$ . In this case, the individual pulse widths will overlap in time to some degree and produce the illusion of a single track in the N-S tubes with ap-

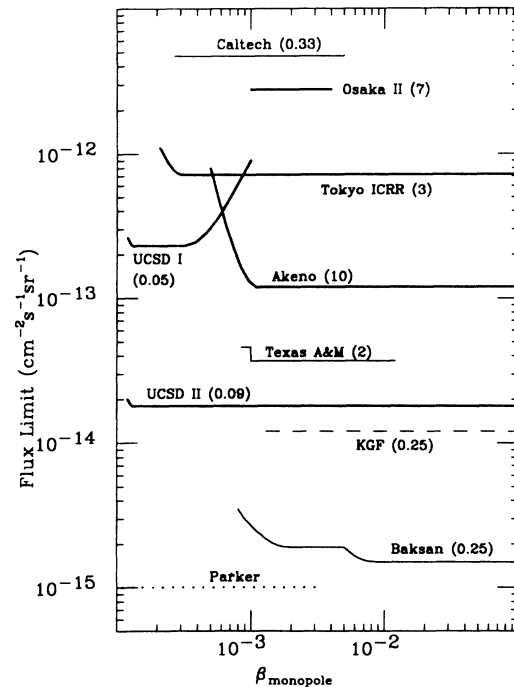


FIG. 8. Selected summary of recent monopole flux limits. Bold lines represent results obtained with proportional wire counter arrays which utilize the DKMPR mechanism. Threshold in units of  $I/I_{\text{min}}$  are noted. Recent limits from scintillator arrays are also shown. The labels correspond to the following references: Caltech (Ref. 6); Osaka (Ref. 19); Tokyo (Ref. 20); UCSD I (University of California, San Diego) (Ref. 15); UCSD II (this work); Akeno (Ref. 21); Texas A&M (Ref. 7); KGF (Kolar Gold Fields) (Ref. 22); Baksan (Ref. 23).

parently large pulse widths. These “multi-CR” events can be easily identified by the presence of two or more separated tracks in the E-W tubes (with normal pulse widths) which match the time of the apparent single track in the orthogonal view. “Showers” are typically discernible as three or more tracks in close proximity viewed in either direction. Whereas the average pulse width along the track is large, the individual pulse widths fluctuate from normal cosmic-ray widths to higher values. “Skew cosmic rays” are single, well-defined tracks in either view, that exhibit a large angle relative to the vertical in the E-W tubes. Hence, the increased path length of the particles within (along) each N-S tube encountered results in larger pulse widths. As before, these “skew CR” events are identified by the normal cosmic-ray widths present in the E-W tubes. “Overlapping cosmic rays” are a limiting case of multiple cosmic rays in which the second track in the E-W tubes is not discernible from the initial track. This results in a single apparent track with large pulse widths in both the N-S and E-W tubes. In addition, all of these events have an implied velocity of  $v > 10^{-2} c$ , which corresponds to the time resolution of the detector.<sup>18</sup> Although the average pulse width in each of these tracks slightly exceeds the “relaxed” filter requirements (recall Fig. 6) for  $\beta > 10^{-2}$ , the pulse widths are still too low ( $\sim 3 \mu\text{s}$ ) to be consistent

with those expected for monopoles in this velocity region. “Malfunctions” are the result of a single abnormally large pulse width within an otherwise normal cosmic-ray track. These invariably came from several suspect tubes in the eighth plane and are easily identified.

#### IV. CONCLUSIONS

For a live time of 578 days, no bare monopole candidates were observed. After correcting for efficiencies, this provides an upper limit on the bare monopole flux (at the 90% confidence level) of  $1.8 \times 10^{-14} \text{ cm}^{-2} \text{ sr}^{-1} \text{ s}^{-1}$  for  $\beta > 1.1 \times 10^{-4}$ . The flux bound set by this experiment is shown in Fig. 8 (labeled as UCSD II), along with limits from other proportional chamber experiments utilizing the DKMPR mechanism, several recent limits from scintillator arrays, and the Parker bound.

#### ACKNOWLEDGMENTS

We are extremely grateful to D. Groom for his assistance in the preparation of Fig. 8. The authors also wish to acknowledge P. Datte, K. Egan, M. Horigan, and J. Masek for assisting with the construction of the detector. This work was supported by the National Science Foundation Grant No. PHY85-17279.

<sup>1</sup>G. 't Hooft, Nucl. Phys. **B79**, 276 (1974); A. Polyakov, Pis'ma Zh. Eksp. Teor. Fiz. **20**, 430 (1974) [JETP Lett. **20**, 194 (1974)].

<sup>2</sup>D. Groom, Phys. Rep. **140**, 323 (1986).

<sup>3</sup>R. Cabrera, Phys. Rev. Lett. **48**, 1378 (1982).

<sup>4</sup>M. S. Turner, E. N. Parker, and T. J. Bogdan, Phys. Rev. D **26**, 1296 (1982).

<sup>5</sup>Recent advances in high- $T_c$  superconductors could open the possibility of large-area induction devices. S. Somalwar, H. Frisch, and J. Incandela, Phys. Rev. D **37**, 2403 (1988).

<sup>6</sup>B. Barish, G. Liu, and C. Lane, Phys. Rev. D **36**, 2641 (1987).

<sup>7</sup>M. Shepko, C. Gagliardi, P. Green, P. McIntyre, T. Meyer, R. Tribble, and R. Webb, Phys. Rev. D **35**, 2917 (1987).

<sup>8</sup>S. Ahlen and G. Tarlé, Phys. Rev. D **27**, 688 (1983).

<sup>9</sup>D. Ficenec, S. Ahlen, A. Marin, J. Musser, and G. Tarlé, Phys. Rev. D **36**, 311 (1987).

<sup>10</sup>S. Drell, N. Kroll, M. Mueller, S. Parke, and M. Ruderman, Phys. Rev. Lett. **50**, 644 (1983).

<sup>11</sup>W. D. Jesse, J. Chem. Phys. **41**, 2060 (1964).

<sup>12</sup>N. M. Kroll and V. Ganapathi, in *Resonance Ionization Spectroscopy and Its Applications, 1984*, proceedings of the Second International Symposium, Knoxville, Tennessee, 1984, edited by G. S. Hurst and M. G. Payne (IOP Conf. Ser. No. 71) (IOP, London, 1984).

<sup>13</sup>L. Bracci, G. Fiorentini, G. Mezzorani, and P. Quarati, Phys. Lett. **143B**, 357 (1984); **155B**, 468(E) (1985).

<sup>14</sup>The percentage of bound states could drop to zero if the monopole is capable of inducing proton decay (Rubakov-Callan effect) as the companion proton would be lost to de-

cay.

<sup>15</sup>G. Masek, L. Knapp, E. Miller, J. Stronski, W. Vernon, and J. White, Phys. Rev. D **35**, 2758 (1987).

<sup>16</sup>C. Mori, M. Uno, and T. Watanabe, Nucl. Instrum. Methods **196**, 49 (1982).

<sup>17</sup>C. Mori and T. Watanabe, Nucl. Instrum. Methods **204**, 149 (1982).

<sup>18</sup>A particle traversing the detector in the vertical direction (0.6 m) in a time less than “1 clock tick” (0.1  $\mu\text{s}$ ) sets an upper limit ( $\beta \approx 10^{-2}$ ) to the velocity that can be accurately determined.

<sup>19</sup>C. Cho, S. Higashi, N. Hiraoka, A. Maruyama, S. Ozaki, T. Sato, T. Suwada, T. Takahashi, H. Umeda, and K. Tsuji in *Proceedings of the 19th International Cosmic Ray Conference*, La Jolla, California 1985, edited by F. C. Jones, J. Adams, and G. M. Mason (NASA Conf. Publ. No. 2376) (Goddard Space Flight Center, Greenbelt, MD, 1985), p. 214.

<sup>20</sup>F. Kajino, S. Matsuno, Y. K. Yuan, and T. Kitamura, Phys. Rev. Lett. **52**, 1373 (1984).

<sup>21</sup>T. Hara *et al.*, Phys. Rev. Lett. **56**, 553 (1986).

<sup>22</sup>M. Krishnaswamy, M. Menon, N. Mondal, V. Narasimham, B. Sreekantan, Y. Hayashi, N. Ito, S. Kawakami, and S. Miyake, in *Proceedings of the 19th International Cosmic Ray Conference* (Ref. 19), p. 234.

<sup>23</sup>E. Alexeyev, M. Boliev, A. Chudakov, and S. Mikheyev, in *Proceedings of the 19th International Cosmic Ray Conference* (Ref. 19), p. 250. The curve shown in Fig. 8 is from the more recent review article by Groom (Ref. 2).